Mechanical Systems and Signal Processing 84 (2017) 499–515

Contents lists available at ScienceDirect

Mechanical Systems and Signal Processing

journal homepage: www.elsevier.com/locate/ymssp

Extracting harmonic signal from a chaotic background with local linear model ☆

Chenlong Li [a], Liyun Su [b,*]

[a] School of Science, Tianjin University, Tianjin 300072, China
[b] School of Mathematics and Statistics, Chongqing University of Technology, Chongqing 400054, China

A R T I C L E I N F O

Article history:
Received 23 February 2016
Received in revised form
14 June 2016
Accepted 25 July 2016
Available online 3 August 2016

Keywords:
Chaotic background noise
Weak harmonic signal
Two-layer local linear model
Detection and estimation

A B S T R A C T

In this paper, the problems of blind detection and estimation of harmonic signal in strong chaotic background are analyzed, and new methods by using local linear (LL) model are put forward. The LL model has been exhaustively researched and successfully applied for fitting and forecasting chaotic signal in many chaotic fields. We enlarge the modeling capacity substantially. Firstly, we can predict the short-term chaotic signal and obtain the fitting error based on the LL model. Then we detect the frequencies from the fitting error by periodogram, a property on the fitting error is proposed which has not been addressed before, and this property ensures that the detected frequencies are similar to that of harmonic signal. Secondly, we establish a two-layer LL model to estimate the determinate harmonic signal in strong chaotic background. To estimate this simply and effectively, we develop an efficient backfitting algorithm to select and optimize the parameters that are hard to be exhaustively searched for. In the method, based on sensitivity to initial value of chaos motion, the minimum fitting error criterion is used as the objective function to get the estimation of the parameters of the two-layer LL model. Simulation shows that the two-layer LL model and its estimation technique have appreciable flexibility to model the determinate harmonic signal in different chaotic backgrounds (Lorenz, Henon and Mackey–Glass (M–G) equations). Specifically, the harmonic signal can be extracted well with low *SNR* and the developed background algorithm satisfies the condition of convergence in repeated 3–5 times.

1. Introduction

Chaos theory has been considered in signal processing for about two decades [1]. Along with the development of the chaos theory, many researchers have found chaos theory may provide a novel tool to signal processing. As we see from recent works on chaos, the applications of chaos to varieties of disciplines have drawn great attention, many researchers are interested in these challenging problems and take many efforts, and there are many applications of chaotic signal processing that have been considered in many different fields [2–12].

☆ This project was supported by Natural Science Foundation Project of China (Grant no. 11471060), Fundamental and Advanced Research Project of CQ CSTC of China (Grant no. cstc2014jcyjA40003), and Scientific and Technological Research Program of Chongqing Municipal Education Commission of China (Grant nos. KJ130818 and KJ130810).

* Corresponding author.
E-mail address: cloudhopping@163.com (L. Su).

http://dx.doi.org/10.1016/j.ymssp.2016.07.040
0888-3270/

An interesting conventional signal processing problem is that the determinate signal is corrupted by noise and we need to extract the signal or reduce the noise. In general, the noise is considered as White Noise. And chaos theory has been found that it could provide an efficient tool to solve this problem. In Ref. [13], Duffing oscillator is used for detecting signal. An array of oscillators have been successfully applied in detection applications [14–16]. On the other hand, in our surrounding, lots of noise have been found chaotic [1–3]. And a variety of researches that the chaotic signal acts as noise in a detection and estimation problem have been done, and the determinate signal that is of direct interest and is corrupted by chaotic noise [4–12]. As many signals possess applications, researchers are interested in extracting the determinate signal, and statistics has been considered as a major tool to perform chaotic signal analysis at first. Then, some researchers applied a nonlinear predictor to model the chaotic signal background and a model-based algorithm is considered to detect the determinate signal in chaotic background [9]. But it is not real advantages in practical applications when compared to the conventional approaches because there is lack of efficient processing techniques to exploit the chaotic properties [1]. For instance, although chaotic signals have chaotic characteristics, chaotic signal processing use conventional concepts such as correlators and do not exploit any chaotic characteristics in many literatures, and there is no doubt that no significant benefit is obtained [1].

A natural approach is to investigate whether the received signal matches the nonlinear map f which generates the chaotic signal, in other words, as chaotic systems are very sensitive to the initial value and if the target signal exists, it will not fit the mapping f well, and it results in relatively large mean-squared error (*mse*) on the estimators. If the nonlinear function f is unknown, we will fit some nonlinear models such as neural networks to the signals in the detection problem [17,18]. In practice, the frequencies could be detected from the fitting error in some researchers' study. However, it is noted that extracting target signal's frequencies in fitting error efficiently is a problem because the nonlinear models break the structure of the target signals, and we cannot ensure that if the frequencies are the same as that of the target signal. In our opinion, to extract target signal efficiently, more chaotic signal processing techniques should be developed. And these techniques should be able to exploit the underlying chaotic characteristics.

In this paper, we investigate a variety of signal processing techniques in which chaotic characteristics have been considered. Based on the short term predictability and sensitivity to initial value, an efficient hybrid processing technique is proposed, which can be used for detecting and estimating of harmonic signal in chaotic noise background that the nonlinear mapping f is unknown. We first consider the problem that detection of harmonic signal in chaotic noise background. We use the LL model to form an approximated model for f. The LL model is one of the local methods using only part of the past information to approximate the local attractor [19]. The future values can be inferred by using the neighborhoods of the current point. For most chaotic time series, the LL model is valid. And the frequencies can be detected from the fitting error, and a property is proved to ensure that they have the similar frequencies. Then a two-layer LL model is proposed to extract the harmonic signal from chaotic background.

The rest of the paper is organized as follows. In Section 2, we will first give a formulation of detection and estimation, as most signal processing problems, which can be categorized into these two functions. Then, we develop an detection technique that has not been proposed in the literature and provide a two-layer LL model for estimating. The results of simulation are reported in Section 3, up-to-date researches on detection and estimation of the harmonic signal are reported, which demonstrate that the proposed methodology has appreciable flexibility to detect and estimate the determinate harmonic signal in strong chaotic background. The conclusion of this paper is given in Section 4.

2. Methodology formulation

We establish a two-layer LL model to estimate the determinate harmonic signal. An exhaustive search is intractable. To solve this, we develop an efficient backfitting algorithm which has been successfully applied for estimating parameters in other models such as the AFAR model. Further we provide a property on the detection problem by using LL models fitting error which has not been addressed before.

The methodology in this section mainly researches three key aspects:

(1) One result on the frequencies in fitting error is derived under some assumptions.
(2) The accuracy of the estimated frequencies of the determinate harmonic signal.
(3) To establish a two-layer LL model and estimate the determinate harmonic signal by the backfitting algorithm.

2.1. Phase space reconstruction and LL model

For a scalar chaotic signal $x(1), x(2), \ldots, x(n)$, the first step of establishing a LL model is the phase space reconstruction. According to Takens' embedding theory [20], the phase space can be reconstructed, and the reconstructed phase points are $X(t) = (x(t), x(t-\tau), \ldots, x(t-(m-1)\tau))'$, where $t = n_1, n_1+1, \ldots, n$ and $n_1 = 1 + (m-1)\tau$. The embedding dimension m and the time delay τ can be obtained by using Cao's method [21]. Then, a continued vector mapping F: $\mathbf{R}^m \to \mathbf{R}^m$ or f: $\mathbf{R}^m \to \mathbf{R}$ can be used to describe the unknown evolution from $X(t)$ to $X(t+1)$ or $x(t+1)$. That is $X(t+1) = F(X(t))$ or $x(t+1) = f(X(t))$. Then, we approximate the mapping f by a LL model. That is,

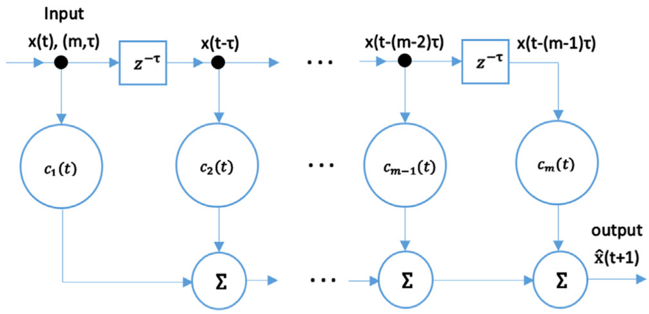

Fig. 1. Local linear (LL) model.

$$g_t(X(t)) = \sum_{j=1}^{m} c_j(t)x(t-(j-1)\tau) = \theta'(t)X(t), \tag{1}$$

where $\theta(t) = (c_1(t), c_2(t), \ldots, c_m(t))'$. This model is displayed in Fig. 1. In order to obtain LL model's parameters at the current state point $X(t)$ in the reconstructed phase space, we select q nearest neighbor points $X(t_i)(i = 1, 2, \ldots, q)$ by using the Euclidean distances $d(j) = \|X(j) - X(t)\|_2$ $(j = n_1, n_1 + 1, \ldots, n-1$ and $j \neq t)$. We can estimate the parameters $\theta(t)$ at the current state point $X(t)$ through the least square equation

$$\min_{\theta(t)\in\mathbf{R}^m} \sum_{i=1}^{q} [x(t_i+1) - g_t(X(t_i))]^2 = \min_{\theta(t)\in\mathbf{R}^m} \sum_{i=1}^{q} [x(t_i+1) - \theta'(t)X(t_i)]^2. \tag{2}$$

Set

$$\chi(t) = \begin{bmatrix} x(t_1) & x(t_1-\tau) & \cdots & x(t_1-(m-1)\tau) \\ x(t_2) & x(t_2-\tau) & \cdots & x(t_2-(m-1)\tau) \\ \vdots & \vdots & \ddots & \vdots \\ x(t_q) & x(t_q-\tau) & \cdots & x(t_q-(m-1)\tau) \end{bmatrix}_{q\times m},$$

$$\tilde{X}(t) = (x(t_1+1), x(t_2+1), \ldots, x(t_q+1))'.$$

It follows from least squares theory that

$$\hat{\theta}(t) = \{\chi'(t)\chi(t)\}^{-1}\chi'(t)\tilde{X}(t). \tag{3}$$

Then we can fit the mapping f, and the fitting error can be obtained. The LL filtering is shown in Fig. 2.

Indeed, we observe that some of the chaotic time series cannot be approximated well by LL model. And in this paper, we focus on studying the harmonic signal in chaotic noise which can be approximated well by LL model. Hence we present the hypothesis (or the prerequisite) that the chaotic noise can be approximated well by LL model.

2.2. Detection method

We first consider the problem of detection of deterministic harmonic signal in chaotic noise. The relative signal processing problem can be formulated as a binary hypotheses problem (H_0: no harmonic signal; H_1: harmonic signal exists). That is,

$$H_0: y(t) = x(t),$$
$$H_1: y(t) = x(t) + s(t), \tag{4}$$

where $y(t)$ is the measured signal, $x(t)$ is the chaotic signal, $s(t)$ is the deterministic harmonic signal and independent of $x(t)$. A natural approach is to investigate whether the received signal match f, in practical, frequencies could be detected from the fitting error. In this paper, we use a LL model to form an approximated model for f. Furthermore, based on the property of below, we think that the detected frequencies of fitting error are as same as that of original signal.

Property of fitting error of LL model: Assume that hypotheses of the prerequisite and H_1 hold, and $s(t) = \sum_{k=1}^{p} A_k \sin(2\pi\omega_k t + \varphi_k)$ are weak signals which is independent of chaotic noise. Then, for g_t defined by LL model obtained by using $y(t)$, one gets:

$$s(t+1) - g_t(S(t)) = \sum_{k=1}^{p} A_k\psi_k(t)\sin(2\pi\omega_k t + \varphi_k + \phi_k(t)), \tag{5}$$

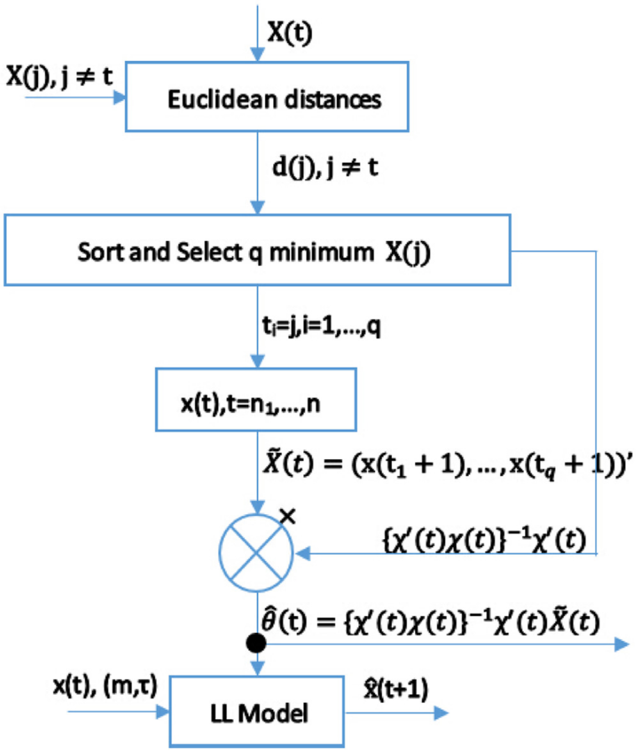

Fig. 2. LL Filtering.

where $S(t) = (s(t), s(t-\tau), \dots, s(t-(m-1)\tau))'$, the embedding dimension m and the time delay τ are obtained by Cao's method, $\psi_k(t)$ and $\phi_k(t)$ change with time.

Proof. We firstly verify the explicit form of $s(t+1) - g_t(S(t))$. According to hypotheses H_1, we have

$$y(t) = x(t) + s(t),$$

where $y(t)$ is the measured signal, $x(t)$ is the chaotic signal and $s(t)$ is the deterministic harmonic signal.

Note that $s(t)$ is the weak signal and independent of chaotic noise, we can reconstruct $y(t)$ with embedding dimension m and time delay τ by Cao's method. Then, we can get the reconstructed phase points

$$Y(t) = (y(t), y(t-\tau), \dots, y(t-(m-1)\tau))' = X(t) + S(t),$$

where $X(t) = (x(t), x(t-\tau), \dots, x(t-(m-1)\tau))'$, $S(t) = (s(t), s(t-\tau), \dots, s(t-(m-1)\tau))'$ and $t = n_1, n_1+1, \dots, n$. Thus, we can establish a LL model. That is,

$$g_t(Y(t)) = \sum_{j=1}^{m} c_j(t) y(t-(j-1)\tau) = \theta'(t) Y(t), \tag{6}$$

where $Y(t) = (y(t), y(t-\tau), \dots, y(t-(m-1)\tau))'$. It follows from Eq. (22) that

$$\hat{\theta}(t) = \{\chi'(t)\chi(t)\}^{-1}\chi'(t)\tilde{Y}(t), \tag{7}$$

where the elements of $\chi(t)$ and $\tilde{Y}(t)$ are replaced by $y(t)$, respectively. Then, we compute

$$s(t+1) - g_t(S(t)) = \sum_{k=1}^{p} A_k[\sin(2\pi\omega_k(t+1) + \varphi_k) - \hat{\theta}'(t)U_k(t)], \tag{8}$$

where $U_k(t) = (\sin(2\pi\omega_k t + \varphi_k), \sin(2\pi\omega_k(t-\tau) + \varphi_k), \dots, \sin(2\pi\omega_k(t-(m-1)\tau) + \varphi_k))$.

Notice that

$$\sin\left(2\pi\omega_k\left(t+1\right) + \varphi_k\right) - \hat{\theta}'(t)U_k(t) = \left(\sum_{j=0}^{m} c_j(t)\gamma_j\right)\sin\left(2\pi\omega_k t + \varphi_k\right) + \left(\sum_{j=0}^{m} c_j(t)\bar{\gamma}_j\right)\cos\left(2\pi\omega_k t + \varphi_k\right), \tag{9}$$

where $c_0(t) \equiv 1$,

$$\gamma_j = \begin{cases} \cos(2\pi\omega_k), & j = 0, \\ -\cos(2\pi\omega_k(j-1)\tau)), & j = 1, 2, \ldots, m, \end{cases} \bar{\gamma}_j = \begin{cases} \sin(2\pi\omega_k), & j = 0, \\ -\sin(2\pi\omega_k(j-1)\tau)), & j = 1, 2, \ldots, m. \end{cases}$$

Then, we have

$$\sin(2\pi\omega_k(t+1) + \varphi_k) - \hat{\theta}'(t)U_k(t) = \psi_k(t)\sin(2\pi\omega_k t + \varphi_k + \phi_k(t)), \tag{10}$$

where $\psi_k(t) = \frac{\Omega'(t)\Upsilon}{|\Omega'(t)\Upsilon|}\sqrt{(\Omega'(t)\Upsilon)^2 + (\Omega'(t)\bar{\Upsilon})^2}$, $\phi_k(t) = \arctan\left(\frac{\bar{\Upsilon}'\Omega(t)}{\Upsilon'\Omega(t)}\right)$, $\Omega(t) = (1, \hat{\theta}'(t))'$, $\Upsilon = (\gamma_0, \gamma_1, \ldots, \gamma_m)'$, $\bar{\Upsilon} = (\bar{\gamma}_0, \bar{\gamma}_1, \ldots, \bar{\gamma}_m)'$.
This completes the proof. □

Note that

$$e(t+1) = y(t+1) - g_t(Y(t)) = x(t+1) + s(t+1) - g_t(X(t)) - g_t(S(t)) = s(t+1) - g_t(S(t)) + \varepsilon(t+1), \tag{11}$$

where $\varepsilon(t+1) = x(t+1) - g_t(X(t))$ are independent of $s(t+1) - g_t(S(t))$. Hence, we consider using periodogram to identify the frequencies of harmonic signal from $e(t)$. Here we assume that $\varepsilon(t)$ cannot affect the detection because of the independence and the large fitting error is caused by $s(t)$. It looks like that the harmonic signal is converted into narrow-band signal by the LL model. And the central frequencies of $s(t+1) - g_t(X(t))$ can be detected by periodogram, which has been considered as a tool to detect frequencies of signal for years, hence, we will no longer introduce it in this paper.

2.3. Two-layer LL model and estimation of harmonic signal

In this section, we think about building a two-layer LL model and estimate the deterministic harmonic signal in chaotic noise. If hypothesis H_1 holds, LL model cannot match the nonlinear mapping f well, hence large fitting error will result. Hypothesis testing can be applied to the fitting error. That is,

$$\begin{aligned} &H_0^*: mse < \delta, \\ &H_1^*: mse > \delta, \end{aligned} \tag{12}$$

where $mse = \frac{1}{n-n_1}\sum_{t=n_1}^{n-1} e^2(t+1)$ is the mean square function of fitting error $e(t+1)$ and δ is the detection threshold. Further, we change the idea to consider this hypothesis testing in Section 2.3.2.

2.3.1. Two-layer LL model

Denote

$$\begin{aligned} &ss(t) = (\cos(2\pi\omega_1 t), \ldots, \cos(2\pi\omega_p t), \sin(2\pi\omega_1 t), \ldots, \sin(2\pi\omega_p t))', \\ &\beta = (a_1, \ldots, a_p, b_1, \ldots, b_p)', \\ &y^*(t) = y(t) - \beta' ss(t), \end{aligned}$$

where ω_i, $i = 1, 2, \ldots, p$ are the detected frequencies from above section and p is the number of frequencies. We use $y^*(t)$ to establish the LL model, and then a two-layer LL model can be established. That is,

$$\begin{cases} y^*(t) = y(t) - \beta' ss(t), \\ y^*(t+1) = g_t(Y^*(t)) = \sum_{j=1}^{m} c_j(t) y^*(t-(j-1)\tau), \end{cases} \tag{13}$$

where $Y^*(t) = (y^*(t), y^*(t-\tau), \ldots, y^*(t-(m-1)\tau))'$. This model is displayed in Fig. 3.

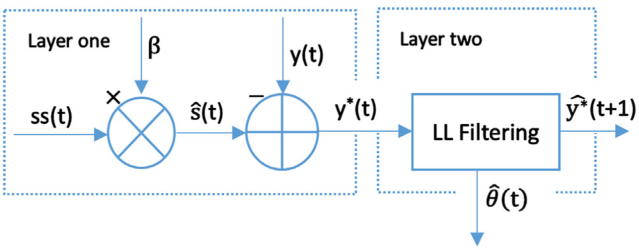

Fig. 3. Two-layer LL model.

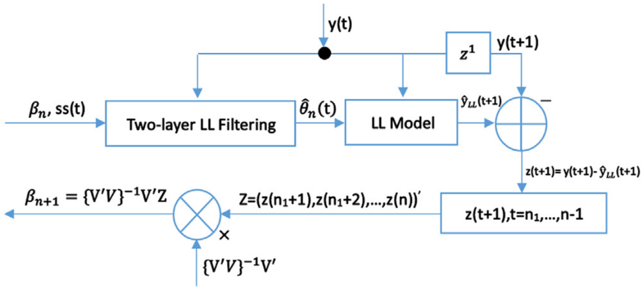

Fig. 4. Backfitting algorithm.

2.3.2. *Estimation method*

The parameters β are selected to against hypothesis H_1^*. Thus, we select the optimal β directly at which the mean-squared error is minimized. That is,

$$\beta = \arg\min_{\beta} \sum_{t=n_1}^{n-1} [y^*(t+1) - \hat{\theta}(t) Y^*(t)]^2, \tag{14}$$

where $\hat{\theta}(t) = \text{argmin}_{\theta(t)} \sum_{i=1}^{q} [y^*(t_i + 1) - \theta(t) Y^*(t_i)]^2$. Then, the estimation of $s(t)$ can be denoted as $\hat{s}(t) = \beta' ss(t)$.

For estimating β, one needs $\theta(t)$ known, however, the estimators of $\theta(t)$ relay on β. An exhaustive research is knotty, thus we follow the backfitting algorithm [22] and develop it to estimate β and $\theta(t)$. Based on the backfitting algorithm, this issue can be split into two parts: estimation of function $g_t(\cdot)$ with given β and estimation of β with given $g_t(\cdot)$. The estimation method is given below and its diagram is displayed in Fig. 4.

(a) *Estimation of LL model with given* β: For given β, we need to estimate

$$\theta(t) = \arg\min_{\theta(t)} \sum_{i=1}^{q} [y^*(t_i + 1) - \theta'(t) Y^*(t_i)]^2, \; t = n_1, \ldots, n-1. \tag{15}$$

With $y^*(t)$, $Y^*(t)$ and $\tilde{Y}^*(t)$ instead of $x(t)$, $X(t)$ and $\tilde{X}(t)$ in Section 2.1, respectively. The estimators $g_t(\cdot)$ can be obtained. That is,

$$\hat{\theta}(t) = \{\chi'(t)\chi(t)\}^{-1}\chi'(t)\tilde{Y}^*(t). \tag{16}$$

(b) *Search for* β*-direction with the* $g_t(\cdot)$ *fixed. For given* $g_t(\cdot)$*, we search for* β *to minimize*

$$R(\beta) = \sum_{t=n_1}^{n-1} [y^*(t+1) - \hat{\theta}'(t) Y^*(t)]^2. \tag{17}$$

Set

$$SS_i^1(t) = (\cos(2\pi\omega_i t), \cos(2\pi\omega_i (t-\tau)), \ldots, \cos(2\pi\omega_i (t-(m-1)\tau))'$$
$$SS_i^2(t) = (\sin(2\pi\omega_i t), \sin(2\pi\omega_i (t-\tau)), \ldots, \sin(2\pi\omega_i (t-(m-1)\tau))'$$

It is easy to see from Eq. (17) that

$$R(\beta) = \sum_{t=n_1}^{n-1} [z(t+1) - \beta' V(t)]^2, \tag{18}$$

where

$$z(t+1) = y(t+1) - \hat{y}_{LL}(t+1),$$
$$\hat{y}_{LL}(t+1) = \hat{\theta}'(t) Y(t),$$
$$V(t) = (\cos(2\pi\omega_1(t+1)) - \hat{\theta}'(t) SS_1^1(t), \ldots, \cos(2\pi\omega_p(t+1)) - \hat{\theta}'(t) SS_p^1(t), \sin(2\pi\omega_1(t+1)) .$$
$$- \hat{\theta}'(t) SS_1^2(t), \ldots, \sin(2\pi\omega_p(t+1)) - \hat{\theta}'(t) SS_p^2(t))'$$

It follows from least squares theory that

$$\hat{\beta} = \{V'V\}^{-1} V' Z, \tag{19}$$

where $V = (V(n_1), V(n_1+1), \ldots, V(n-1))$, $Z = (z(n_1+1), z(n_1+2), \ldots, z(n))'$.

2.3.3. The convergence conditions

In this subsection, we shall give the convergence conditions of the process of successive approximations of items (a) and (b).

In item (a), in order to estimate $\theta_k(t)$ with given β_k, one needs to minimize

$$mse_{a,\beta_k}(\theta(t)) = \sum_{i=1}^{q} [y^*(t_i+1) - \theta'(t)Y^*(t_i)]^2,\ t = n_1, \ldots, n-1. \tag{20}$$

Set

$$\tilde{S}_1(t) = (s(t_1+1), s(t_2+1), \ldots, s(t_q+1))',$$
$$\tilde{S}_2(t) = (S(t_1), S(t_2), \ldots, S(t_q))_{m\times q},$$
$$SS(t) = (ss(t), ss(t-\tau), \ldots, ss(t-(m-1)\tau))_{2p\times m}$$
$$\chi_2(t) = (ss(t_1+1), ss(t_2+1), \ldots, ss(t_q+1))_{2p\times q},$$
$$\chi_3(t) = (SS'(t_1)\beta_k, SS'(t_2)\beta_k, \ldots, SS'(t_q)\beta_k)_{m\times q}.$$

Substituting $y^*(t) = y(t) - \beta' ss(t)$ and $y(t) = x(t) + s(t)$ into Eq. (20), one gets

$$mse_{a,\beta_k}(\theta(t)) = \| \tilde{X}(t) + \epsilon(t) - \theta'(t)(\chi(t) + \xi(t)) \|_2^2, \tag{21}$$

where $\epsilon(t) = \tilde{S}_1(t) - \beta_k'\chi_2(t)$ and $\xi(t) = \tilde{S}_2(t) - \chi_3(t)$.

In item (b), in order to estimate β_{k+1} with given $\theta_k(t)$, we need to minimize

$$mse_{b,\theta_k(t)}(\beta) = \| \tilde{X} - \Theta_k(X) + \tilde{S} - \Theta_k(S) - (\chi_2' - \Theta_k(SS))\beta \|_2^2, \tag{22}$$

where

$$\theta_k(t) = (c_{1,k}(t), c_{2,k}(t), \ldots, c_{m,k}(t))',$$
$$\tilde{X} = (x(n_1+1), x(n_1+2), \ldots, x(n))',$$
$$\tilde{S} = (s(n_1+1), s(n_1+2), \ldots, s(n))',$$
$$\Theta_k(X) = (\theta_k'(n_1)X(n_1), \theta_k'(n_1+1)X(n_1+1), \ldots, \theta_k'(n-1)X(n-1))',$$
$$\Theta_k(S) = (\theta_k'(n_1)S(n_1), \theta_k'(n_1+1)S(n_1+1), \ldots, \theta_k'(n-1)S(n-1))',$$
$$\chi_2 = (ss(n_1+1), ss(n_1+2), \ldots, ss(n))_{2p\times(n-n_1)},$$
$$\Theta_k(SS) = (\theta_k'(n_1)SS'(n_1); \theta_k'(n_1+1)SS'(n_1+1); \cdots; \theta_k'(n-1)SS'(n-1))_{(n-n_1)\times 2p}.$$

Denote

$$\varepsilon = \tilde{X} - \Theta_k(X),$$
$$\tilde{S}^+ = (s(n_1), s(n_1+2), \ldots, s(n))',$$
$$E = \begin{bmatrix} 0 & 0_{1\times(n-n_1)} \\ 0_{(n-n_1)\times 1} & I_{(n-n_1)\times(n-n_1)} \end{bmatrix},$$
$$\alpha_{i,j} = \begin{cases} c_{m-\frac{(j-i)}{\tau},n}(n_1+i-1), j = i, i+\tau, \ldots, i+(m-1)\tau, i = 1, 2, \ldots, n-n_1, \\ 0, j \neq i, i+\tau, \ldots, i+(m-1)\tau, i = 1, 2, \ldots, n-n_1+1, \end{cases}$$
$$\Xi = (\alpha_{i,j})_{(n-n_1+1)\times(n-n_1+1)},$$
$$\chi_s^+ = (ss(n_1), ss(n_1+1), \ldots, ss(n))_{2p\times(n-n_1+1)}.$$

Then we have

$$mse_{b,\theta_k(t)}(\beta) = \| \varepsilon + (E - \Xi)\tilde{S}^+ - (E - \Xi)\chi_s^{+\prime}\beta \|_2^2, \tag{23}$$

Compared with the original optimization objectives below

$$mse_a(\theta(t)) = \| \tilde{X}(t) - \theta'(t)\chi_1(t) \|_2^2, \tag{24}$$

$$mse_b(\beta) = \| \tilde{S}^+ - \chi_s^{+\prime}\beta \|_2^2, \tag{25}$$

it can be seen that the optimization objectives (Eqs. (21) and (23)) are disturbed by a jamming. If the jamming is weak, the solutions of optimizing objectives (Eqs. (21) and (23)) can be treated as a suboptimum solutions of optimizing objectives (Eqs. (24) and (25)), respectively.

In fact, since $s(t)$ is the weak signal, we select 0 as the initial value of β. And the meaning of weak in Eq. (21) can be defined by the $SNR(t)$ (signal-to-noise ratio). That is,

$$SNR_1(t) = 10\log_{10}\left(\frac{\|\tilde{S}_1(t)\|_2^2}{\|\tilde{X}(t)\|_2^2}\right) \le \triangle_1, \quad SNR_2(t) = 10\log_{10}\left(\frac{\|\tilde{S}_2(t)\|_F^2}{\|\chi_1(t)\|_F^2}\right) \le \triangle_1', \tag{26}$$

where matrix norm $\| A \|_F = \left(\sum_{i=1}^{m} \sum_{j=1}^{n} (a_{ij}^2) \right)^{1/2}$ is the Frobenius norm, $t = n_1, n_1 + 1, \ldots, n - 1$. For the data with sample size $n - n_1$, we have

$$SNR = 10\log_{10}\left(\frac{\|\tilde{S}_1\|_2^2}{\|\tilde{X}\|_2^2}\right). \tag{27}$$

Since $t = n_1, n_1 + 1, \ldots, n - 1$ take almost all points and the local points are selected by Euclidean distance, one can conjecture that the SNR has a relationship with $SNR(t)$: suppose the sum of $\|\tilde{S}_1(t)\|_2^2$ for all t and that of $\|\tilde{X}(t)\|_2^2$ are respectively q times $\|\tilde{S}_1\|_2^2$ and $\|\tilde{X}\|_2^2$ where q is the number of local points. Then we have $q\|\tilde{S}_1\|_2^2 = \sum_{t=n_1}^{n-1} \|\tilde{S}_1(t)\|_2^2 \le 10^{\frac{\triangle_1}{10}} \sum_{t=n_1}^{n-1} \|\tilde{X}(t)\|_2^2 = 10^{\frac{\triangle_1}{10}} q \|\tilde{X}\|_2^2$. And $qm\|\tilde{S}_2\|_2^2 = \sum_{t=n_1}^{n-1} \|\tilde{S}_2(t)\|_F^2 \le 10^{\frac{\triangle_1'}{10}} \sum_{t=n_1}^{n-1} \|\chi_1(t)\|_F^2 = 10^{\frac{\triangle_1'}{10}} qm\|\tilde{X}\|_2^2$ holds under the similar assumption. That is,

$$SNR \le \min\{\triangle_1, \triangle_1'\}. \tag{28}$$

If inequation (28) holds with the same assumptions above, one gets

$$Mean\left(\sum_{t=n_1}^{n-1} SNR_1(t)\right) \le \triangle_1, \quad Mean\left(\sum_{t=n_1}^{n-1} SNR_2(t)\right) \le \triangle_1', \tag{29}$$

which means that the upper bound $\triangle_{1,1}$ of SNR should be less than $\min\{\triangle_1, \triangle_1'\}$ to ensure most of the $SNR_1(t)$ and $SNR_2(t)$ at point t less than $\triangle_1$ and $\triangle_1'$, respectively. It depends on the variances of $SNR_1(t)$ and $SNR_2(t)$. Now, for the first iteration, the optimal solution of minimum (Eq. (21)) in term (a) can be treated as a suboptimum solution of minimum Eq. (24).

For Eq. (23), the meaning of weak can be defined by the SNR_1. That is,

$$SNR_1 = 10\log_{10}\left(\frac{\|\varepsilon\|_2^2}{\|(E - \Xi)\tilde{S}^+\|_2^2}\right) \le \triangle_2. \tag{30}$$

Using the matrix norm, one gets $\|\varepsilon\|_2^2 \le 10^{\frac{\triangle_2}{10}} \|(E - \Xi)\tilde{S}^+\|_2^2 \le 10^{\frac{\triangle_2}{10}} \|(E - \Xi)\|_F^2 \|\tilde{S}^+\|_2^2$ and

$$SNR \ge -\triangle_2 + 10\log_{10}\left(\frac{\|\varepsilon\|_2^2}{\|(E - \Xi)\|_F^2 \|\tilde{X}\|_2^2}\right), \tag{31}$$

in which the point at $t = n_1$ is ignored (the same below). Let $\triangle_{3,1} = -\triangle_2 + 10\log_{10}\left(\frac{\|\varepsilon\|_2^2 \|\tilde{S}^+\|_2^2}{\|\tilde{X}\|_2^2 \|(E-\Xi)\tilde{S}^+\|_2^2}\right)$, and $SNR \ge \triangle_{3,1}$, one gets inequation (30). Note that the unknown sine signal can be expressed as $\beta_{true}' ss(t)$ where β_{true}' is the truth-value. Let $\beta = \beta_{true}$ with condition

(**A1**): The frequencies of sine signal are known, one gets $\|(E - \Xi)\tilde{S}^+ - (E - \Xi)\chi_s^+\beta\|_2^2 = \|\tilde{S}^+ - \chi_s^+\beta\|_2^2 = 0$. Hence the optimal solution of minimum Eq. (23) in term (b) can be treated as suboptimum solution of Eq. (25) under condition $SNR \ge \triangle_{3,1}$.

Here we summarize the analysis. In the initial iteration of item (a), we take $\beta = \beta_1 = 0$. Under condition.

(**A2.1**): $SNR \le \triangle_{1,1}$, one gets $\theta_1(t) = \mathrm{argmin}_{\theta(t)} mse_{a,\beta_1}(\theta(t))$. In the initial iteration of item (b), we take $\theta(t) = \theta_1(t)$. Under condition.

(**A3.1**): $SNR \ge \triangle_{3,1}$, one gets $\beta_2 = \mathrm{argmin}_{\beta} mse_{b,\theta_1(t)}(\beta)$ which is a suboptimum solution of the optimization objective equation (25). In the second iteration of item (a), we take $\beta = \beta_2$. Under the condition **(A2.2):** $SNR \le \triangle_{1,2}$ and the prerequisite condition.

(**A4**): The less jamming in chaotic signal, the more prediction accuracy of chaotic signal can be obtained by LL model, that is, if $mse_{b,\theta_1(t)}(\beta_2) \le mse_{b,\theta_1(t)}(\beta_1)$, then $mse_{b,\theta_2(t)}(\beta_2) \le mse_{b,\theta_1(t)}(\beta_1)$, where $\triangle_{1,2}$ is a new upper bound that makes inequation (26) holds and $\theta_2(t) = \mathrm{argmin}_{\theta(t)} mse_{a,\beta_2}(\theta(t))$. In the second iteration of item (b), we take $\theta(t) = \theta_2(t)$. Under condition.

(**A3.2**): $SNR \ge \triangle_{3,2}$, where $\triangle_{3,2}$ is a new lower bound that makes inequation (30) holds, one gets $mse_{b,\theta_2(t)}(\beta_3) \le mse_{b,\theta_2(t)}(\beta_2)$ in which $\beta_3 = \mathrm{argmin}_{\beta} mse_{a,\theta_2(t)}(\beta)$. Which means β_3 is a better suboptimum solution of the optimization objective equation (25) than β_2. Thus, by using condition (**A4**) again, and conditions {(**A2.k**)} and {(**A3.k**)} hold in the following iteration, one gets

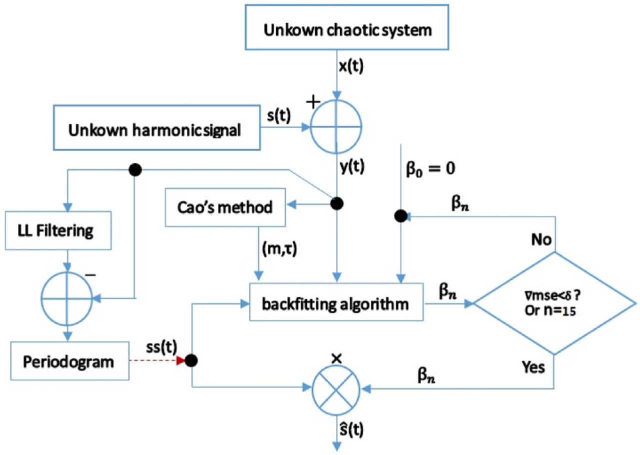

Fig. 5. Two-layer LL filtering algorithm.

$$mse_{b,\theta_k(t)}\left(\beta_k\right) \le \cdots \le mse_{b,\theta_2(t)}\left(\beta_2\right) \le mse_{b,\theta_1(t)}\left(\beta_1\right). \tag{32}$$

Then the algorithm is convergent and one gets a series of $\{\triangle_{1,k}\}$ and $\{\triangle_{3,k}\}$. For *SNR*, there is a upper bound denoted by $\triangle_1^* = \max\{\triangle_{1,1}, \triangle_{1,2}, \ldots, \triangle_{1,k}\}$ and a lower bound $\triangle_3^* = \min\{\triangle_{3,1}, \triangle_{3,2}, \ldots, \triangle_{3,k}\}$ to ensure all {(**A2.k**)} and {(**A3.k**)} hold. So these conditions can be replaced by conditions (**A2**): $SNR \le \triangle_1^*$ and (**A3**): $SNR \ge \triangle_3^*$, respectively. And in the meaning that $mse_{b,\theta_{k-1}(t)}(\beta_k) \le mse_{b,\theta_{k-1}(t)}(\beta_{k-1})$, the β_k is estimated better than β_{k-1}.

Remark 1. Eq. (28) shows that the *SNR* needs a upper bound. Eq. (31) shows that the *SNR* needs a lower bound. Since β_1 is selected and β_2 is a suboptimum solution, it can be seen that the first $nmse_1$ should be small and the second mse_2 where $mse_k = \frac{1}{n-n_1} mse_{b,\theta_k(t)}(\beta_k)$ should be rapid reduce. One can see these in Fig. 8 in Example 2. On the other hand, we first detect the frequencies of sine signal from the fitting error by periodogram with high accuracy so that the condition (**A1**) holds. If the sine signal is proper weak, the conditions (**A2**) and (**A3**) hold. The condition (**A4**) is a prerequisite condition, which is compatible with the prerequisite condition.

(**A5**): The chaotic signal is well approximated by LL model, that is, $\| \varepsilon \|_2^2$ is small.

2.4. Performance of algorithm

We now outline the algorithm. Fig. 5 presents the algorithm diagram.

Step 1: For a scalar time series $y(t)$, $t = 1, 2, \ldots, n-1$, reconstruct phase space with the embedding dimension m and the time delay τ.

Step 2: Compute the Euclidean distances and select the nearest q points.

Step 3: Establish LL model and identify the frequencies from fitting error by using periodogram.

Step 4: Specify an initial value of β, repeat (a) and (b) below until two successive values of β defined in Eq. (14) differ insignificantly.

(1) For a given β, estimate $g_t(\cdot)$ by Eq. (16).
(2) For given $g_t(\cdot)$, estimate β by Eq. (19).

Step 5: Fit $s(t)$ with the obtained $\hat{\beta}$ in step 4.

Some additional remarks are now in order.

Remark 2.

i. The embedding dimension m and the time delay τ can be obtained by the autocorrelation function method and Cao's method in step 1, and we let the number of nearest points $q = 2m + 1$ in step 2.
ii. We extract the determinate signal in step 4, there are some key aspects:

(1) Denote $\hat{\omega}_k$ are estimation of ω_k, and they are not the same. As $t \to \infty$, it will cause a sufficiently large error for a sine function. Then, the estimation of β in step 4 may not be estimated well because of the error. In order to solve this problem, for $y(t)$ with data size T, we search for ω_k further in step 4. We let $\hat{\omega}_k$ change $\nabla\omega = 10^{-k}$ where $k > 1 + \log_{10}(T)$ each time in the interval $[\hat{\omega}_k - \delta, \hat{\omega}_k + \delta]$ to ensure the estimation of β in step 4 is convergent. We let δ=0.1 in terms of the examples reported in Section 3. Further the $\hat{\omega}_k^*$ can be selected with the minimization *mse*.

(2) We expect that the estimator derived will be good if the initial value of β is reasonably good. Note that $s(t)$ is weak signal, we select 0 as the initial value of the β. Because Cao's method has antinoise ability and the independence of $s(t)$ which is also weak signal, the embedding dimension and the time delay are not necessarily recomputed and the Euclidean distances does not need to be calculated again when the β is iterated.

iii. After obtaining embedding dimension and time delay, we select sample size to reduce the computational error when the frequencies are estimated. For example, we have data with sample size 5000 and embedding dimension and the time delay are repetitive m and τ, we select data with sample size $4001 + (m - 1)\tau$ to estimate frequencies.

Remark 3.

i. To speed up the computation further, we can use parallel computing technique in step 4.
ii. In particular, the $y(t)$ with data size T can be split into M parts with enough number to ensure the accuracy of the estimation of β, such that we can speed up the computation and amend the estimation of phase of the deterministic harmonic signal. For implementing this technique, the formulation of Eq. (18) should be rewritten as

$$R(\beta_i) = \sum_{t=n_i}^{n_{i+1}-1} [z(t+1) - \beta_i' V(t)]^2, \quad i = 1, 2, \ldots, M,$$

where $n_i = n_1 + \left[\frac{n-n_1}{M}\right](i-1)$, $i = 1, 2, \ldots, M$, $[\cdot]$ said rounding and $n_{M+1} = n$. The parameters β_i can be estimated:

$$\hat{\beta}_i = \{V_i' V_i\}^{-1} V_i' Z_i,$$

where $V_i = (V(n_i), V(n_i+1), \ldots, V(n_{i+1}-1))$, $Z_i = (z(n_i+1), z(n_i+2), \ldots, z(n_{i+1}))'$. Then we can obtain $\hat{s}(t) = \hat{\beta}_i ss(t)$, $t \in \left[n_i, n_{i+1}-1\right]$ in steps 4 and 5. Furthermore, we can use low accuracy of $\nabla\omega$ to obtain high accuracy of estimation of $s(t)$ by using this technique. We shall illustrate this in Example 3.

3. Simulation

Here, for the finite sample, we demonstrate the performance of the two-layer LL model by the fitting error and the *SNR* in below examples. Three different equations (Lorenz, Henon and M–G equations) are considered to generate chaotic signals as background noises. We mainly investigate two key aspects:

(1) Detection of frequencies of the deterministic harmonic signal and the performance with different *SNR*s and chaotic backgrounds.
(2) Estimation of the deterministic harmonic signal and the performance with different *SNR*s and chaotic backgrounds.

Later, some results about these two aspects are reported in Example 1 and Examples 2–5, respectively.

The *SNR* can be described as follows

$$SNR = 10 \log_{10}\left(\frac{\sigma_s^2}{\sigma_x^2}\right), \tag{33}$$

where σ_s^2 and σ_x^2 are quadratic sum of $s(t)$ and $x(t)$, respectively. The $mse(y)$ is defined as Eq. (31). Cause the harmonic signal is weak, we use the normalized mean square error, that is $nmse(s) = mse(s)/var(s)$, to describe the performance of estimation of harmonic signal.

The Lorenz chaotic signal can be produced as follows [23]:

$$\begin{cases} \dot{x} = \sigma(y - x), \\ \dot{y} = (r - z)x - y, \\ \dot{z} = xy - bz, \end{cases} \tag{34}$$

where σ, r and b are dimensionless parameters and mostly commonly selected to be $\sigma = 10$, $r = 28$ and $b = 8/3$. The standard fourth-order Runge–Kutta method is used to get the Lorenz chaotic signal and the x-coordinate is used for simulation.

Henon mapping is an evident dynamic system [24]. Its equations are written by

$$\begin{cases} x(t+1) = 1 - ax(t)^2 + y(t), \\ y(t+1) = bx(t), \end{cases} \tag{35}$$

where $a = 1.4$ and $b = 0.3$.

The M–G equation has been used in the literature as a benchmark model due to its chaotic characteristics [25]. M–G time series can be generated by the following discrete form:

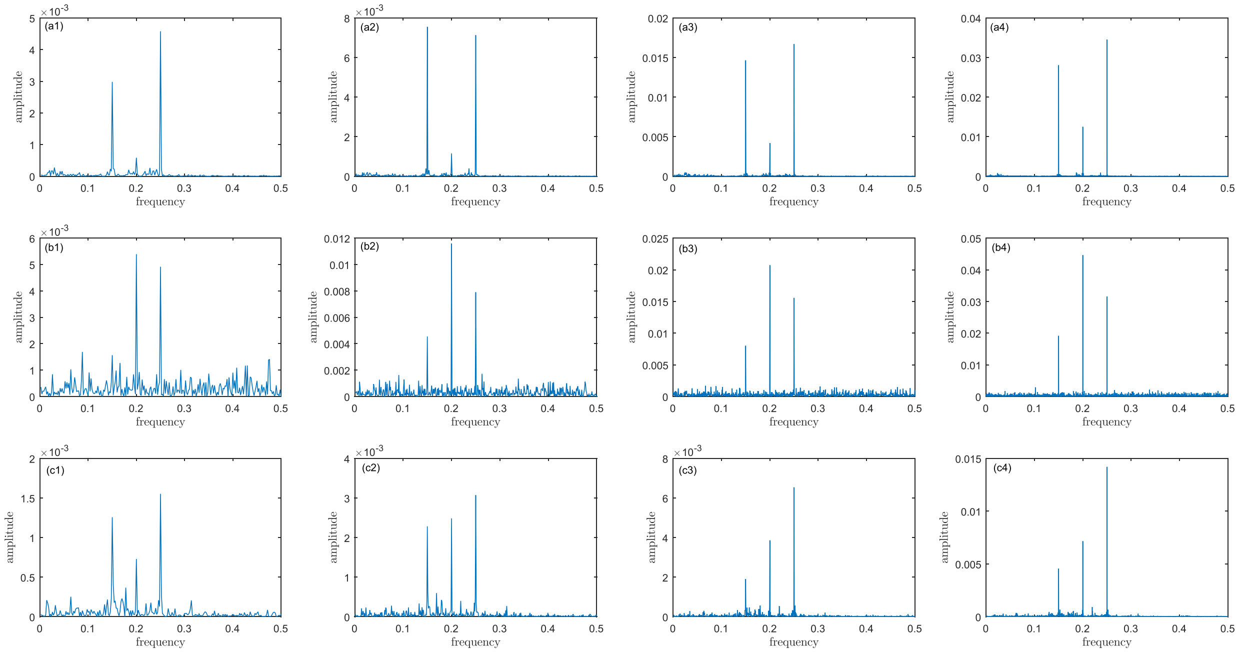

Fig. 6. Simulation results for Example 1: (a1)–(a4) periodograms of fitting error of mixed harmonic and Lorenz signals with sample size 500, 1000, 2000 and 4000, respectively; (b1)–(b4) and (c1)–(c4) show that of mixed harmonic and Henon, M–G signals, respectively.

$$x(t+1) = (1-b)x(t) + \frac{ax(t-\tau)}{1+x(t-\tau)^{10}}, \tag{36}$$

where a=0.2, b=0.1 and τ=17, initial conditions $x(t)|_{t\le 0} = 1.2$.

Then we can get the mixed-signal $y(t) \triangleq x(t) + s(t)$ by using above equations in Examples 1–5.

3.1. Example 1

Consider the harmonic signal

$$s(t) = \sum_{k=1}^{3} A_k \sin(2\pi\omega_k t + 1), \tag{37}$$

where $A_1 = 0.003$, $A_2 = 0.005$, $A_3 = 0.007$, $\omega_1 = 0.25$, $\omega_2 = 0.15$, $\omega_3 = 0.2$.

We compute that the embedding dimensions are 6, 4, 6 and the time delays are 7, 1, 6 of the mixed harmonic and Lorenz, Henon, M–G signals, respectively. Then the mixed signals are selected with sample size 4036, 4004 and 4031, respectively. The results are summarized in Fig. 6. Figs. 6(a1)–(a4) display periodograms of fitting error of mixed harmonic and Lorenz signals with sample size 500, 1000, 2000 and 4000, respectively. Figs. 6(b1)–(b4) and 6(c1)–(c4) show the results of mixed harmonic and Henon, M–G signals, respectively. It can be seen that the frequencies are detected more and more accurate with the increase of sample size. For different *SNR*s, by using Eq. (38) with respective sample size 4036, 4004 and 4031 in Example 4, we got the results that are displayed in Table 1. From Table 1, it can be seen that the frequencies can be detected from fitting error of the mixed harmonic and Lorenz signal in the range from −171.03 dB to −74.47 dB, that of the mixed harmonic and Henon signal in the range from −156.39 dB to −59.81 dB, and that of the mixed harmonic and M-G signal in the range from −160.90 dB to −64.36 dB.

3.2. Example 2

The harmonic signal is generated by Eq. (37). Consider that we obtain $\omega_1 \in [0.24, 0.26]$, $\omega_2 \in [0.14, 0.16]$ and $\omega_3 \in [0.19, 0.21]$. As we note in Remark 1 ii(1), we let $\nabla\omega = 10^{-k}$ where $k = 5 > 1 + \log_{10}(t)$ to select frequencies more accurately. Here, we conducted three simulations with

$$\omega_1 = 0.25, \quad \omega_2 = 0.15, \quad \omega_3 = 0.2$$
$$\omega_1 = 0.2501, \quad \omega_2 = 0.1501, \quad \omega_3 = 0.2001$$
$$\omega_1 = 0.25001, \quad \omega_2 = 0.15001, \quad \omega_3 = 0.20001$$

to illustrate Remark 1 (ii). From Fig. 7, we can see that both the harmonic signals of three groups can be extracted. The performance of extracting the harmonic signal depends on the accuracy of estimation of the frequencies. Furthermore, from Fig. 8, we can see that *mse* satisfies the condition of convergence in repeated 3–5 times. And the *nmse* of the harmonic signals in Fig. 8 is convergent if the accuracy of the estimated frequencies are obtained accurately. Otherwise, they may not be convergent. Note that we use the *mse* of the mixed signals to determine the convergence of the algorithm, and the *nmse* of the harmonic signals is displayed to show the performance and it generally cannot be obtained. On the other hand, from (a3), (b3) and (c3) of Fig. 8, for the estimated frequencies with no error, we can see that the frequencies cannot be detected from the fitting error of $y(t) - \hat{s}(t)$. Which means that the harmonic signals can be counteracted by adding minus $\hat{s}(t)$. And from (a6), (a9), (b6), (b9), (c6) and (c9) of Fig. 8, one can see that the frequencies can still be detected from the fitting error of $y(t) - \hat{s}(t)$ with the estimated frequencies that have errors. Which means that the harmonic signals are still residual by adding minus $\hat{s}(t)$. In addition, from (a4), (b4), and (c4) of Fig. 8, we can see that the obtained *mse* is larger than that obtained with other estimated frequencies. And we should choose the frequencies that lead to minimize the *mse* as estimators.

3.3. Example 3

Example 3 concerns the Remark 3 (ii), which forms an efficient technique to speed up the computation and amend the estimation of phase of the deterministic harmonic signal. The harmonic signal is still generated by Eq. (37).

Set $\omega_1 = 0.2501$, $\omega_2 = 0.1501$, $\omega_3 = 0.2001$ and $M=20$. Thus, reduce the error caused by $\hat{\omega}_k$ from $\sin(4000{*}0.0001\pi)$ to

Table 1
Simulation results for Example 1: varied amplitude.

SNR	Lorenz			*SNR*	Henon			*SNR*	M-G		
	$\omega_1, \omega_2, \omega_3$ (out of order)				$\omega_1, \omega_2, \omega_3$ (out of order)				$\omega_1, \omega_2, \omega_3$ (out of order)		
−267.60	0.0355	0.0423	0.0770	−220.76	0.3863	0.3345	0.3850	−225.28	0.0195	0.0683	0.0200
−235.41	0.0355	0.0423	0.0770	−188.57	0.4570	0.2965	0.2500	−193.09	0.2500	0.0195	0.2000
−203.22	0.2500	0.2000	0.0770	−156.39	0.2500	0.2000	0.1500	−160.90	0.2500	0.2000	0.1500
−171.03	0.2500	0.2000	0.1500	−124.20	0.2500	0.2000	0.1500	−128.71	0.2500	0.2000	0.1500
−138.85	0.2500	0.1500	0.2000	−92.01	0.2500	0.1500	0.2000	−96.52	0.2500	0.2000	0.1500
−106.66	0.1500	0.2500	0.2000	−59.81	0.2500	0.1500	0.2000	−64.36	0.2500	0.1500	0.2000
−74.47	0.1500	0.2500	0.2000	−27.63	0.1500	0.2500	0.3000	−32.15	0.2500	0.2123	0.1500
−42.28	0.1500	0.1633	0.2500	4.56	0.1630	0.0690	0.3888	0.04	0.0670	0.1100	0.0633
−10.09	0.1500	0.0258	0.0283	36.75	0.0528	0.0405	0.0605	32.23	0.4410	0.4455	0.0633

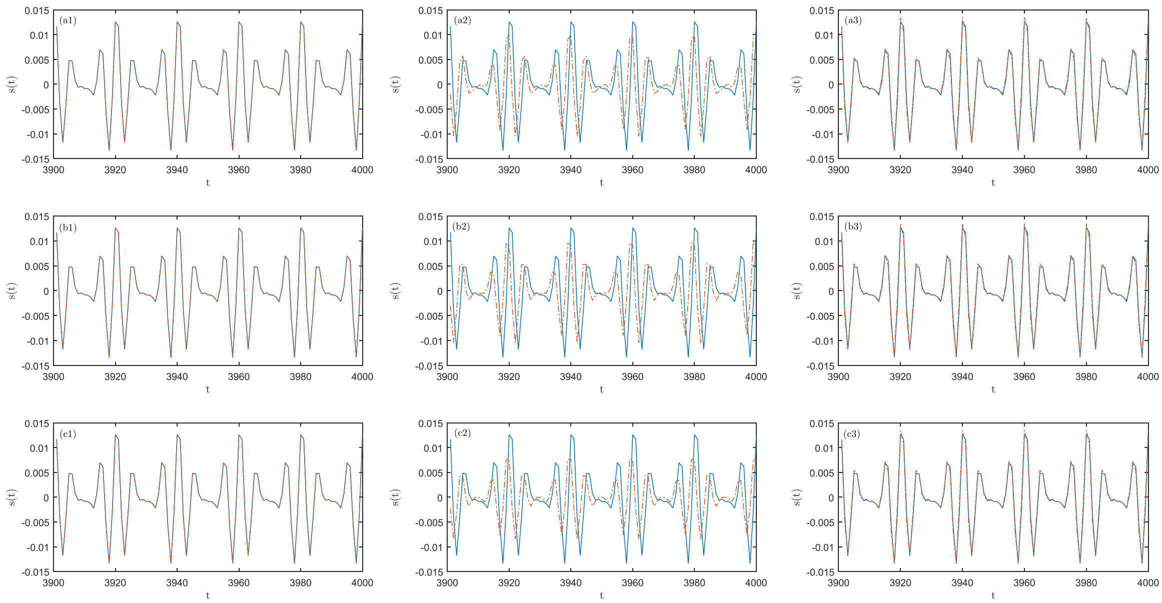

Fig. 7. Simulation results for Example 2 (estimated signal (-·) and the real signal (-)): (a1)–(a3) extracting results from the mixed Lorenz and harmonic signal with $(\omega_1, \omega_2, \omega_3) = (0.25, 0.15, 0.2)$, $(\omega_1, \omega_2, \omega_3) = (0.2501, 0.1501, 0.2001)$, $(\omega_1, \omega_2, \omega_3) = (0.25001, 0.15001, 0.20001)$, respectively; (b1)–(b4) and (c1)–(c4) display the estimation results of the mixed harmonic and Henon, M–G signals, respectively.

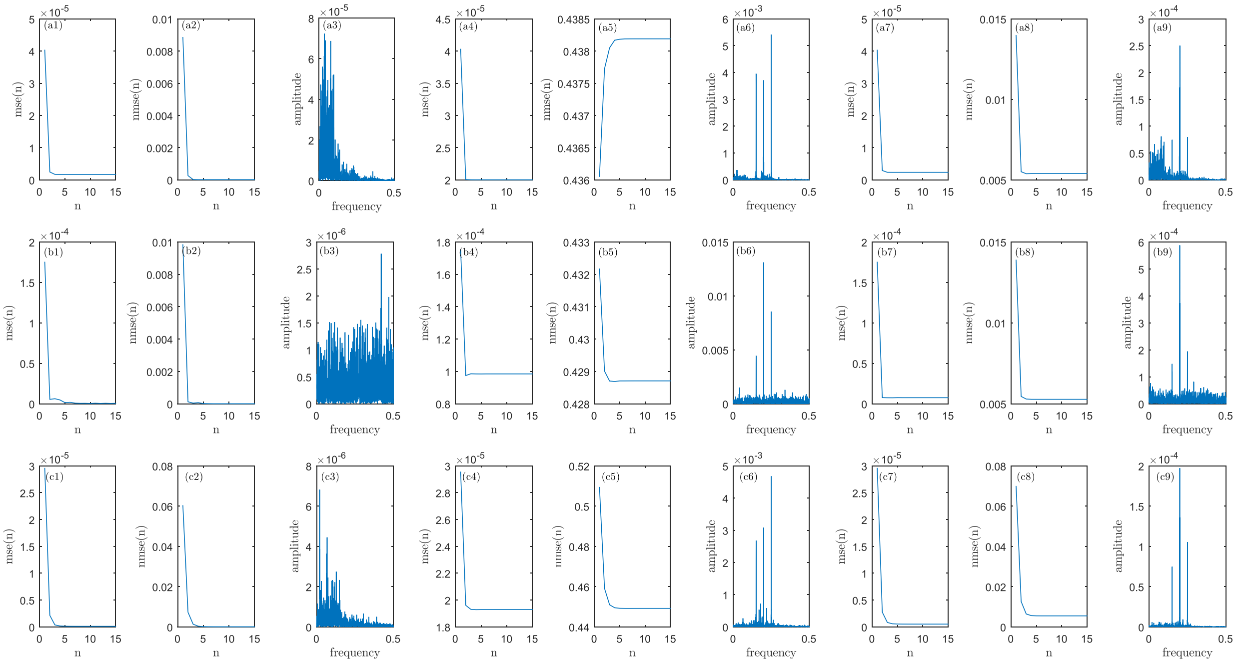

Fig. 8. Simulation results for Example 2: (a1), (a4) and (a7) iteration results of *mse* of the mixed Lorenz and harmonic signal with $(\omega_1, \omega_2, \omega_3) = (0.25, 0.15, 0.2)$, $(\omega_1, \omega_2, \omega_3) = (0.2501, 0.1501, 0.2001)$, $(\omega_1, \omega_2, \omega_3) = (0.25001, 0.15001, 0.20001)$, respectively; (a2), (a5) and (a8) iteration results of *nmse* of harmonic signal with the three groups of frequencies; (a3), (a6) and (a9) periodograms of fitting error of the Lorenz and harmonic signal minus estimation of harmonic signal with the three groups of frequencies, respectively; (b1)–(b9) and (c1)–(c9) display the results of the mixed harmonic and Henon, M–G signals, respectively.

$\sin(200*0.0001\pi)$. The extracted results of the last part of three mixed signals are shown in Fig. 9. Comparing with Figs. 7 and 8, we can see that the harmonic signal can be extracted well. The *mse* of the mixed signals is convergent in repeated 3–5 times. And the *nmse* of the harmonic signals in Fig. 9 is convergent even if the accuracy of the estimated frequencies is obtained not accurately. And the frequencies cannot be detected from the mixed signals minus estimation of harmonic signals with the estimated frequencies that have errors.

3.4. Example 4

We consider the harmonic signal with different parameters

$$s(t) = \sum_{k=1}^{3} A_k(j)\sin(2\pi\omega_k t + 1), \tag{38}$$

where $(\omega_1, \omega_2, \omega_3)$ takes $W_1 \triangleq (0.25, 0.15, 0.2)$ or $W_2 \triangleq (0.2501, 0.1501, 0.2001)$, and $A_k(j) = 0.00001 + 0.00001(5^{j-1} - 1)$, $j = 1, 2, \ldots, 9$ and $k = 1, 2, 3$.

For different harmonic signals in the same chaotic background, we use the same embedding dimensions and time delays as above since Cao's method has antinoise ability. The extracted results with varied amplitudes are summarized in Table 2. We use the original algorithm to estimate the harmonic signal with the accurate estimated frequencies and the advanced version to obtain the harmonic signal with the low accurate estimated frequencies. From Table 2, for the accurate estimated frequencies, it can be seen that the frequencies can be extracted from fitting error of the mixed harmonic and Lorenz, Henon and M–G signals in the range from −203.22 dB to −42.28 dB, −220.76 dB to −59.81 dB, and −160.90 dB to −64.36 dB, respectively; for the low accurate estimated frequencies, it can be seen that the frequencies can be extracted from fitting error of the three mixed signals in the range from −171.03 dB to −42.28 dB, −156.39 dB to −59.81 dB, and −128.71 dB to −64.36 dB, respectively.

3.5. Example 5

Although Cao's method has antinoise ability, it may cause small difference, larger or smaller, for embedding dimension and delay of the same mixed signal because of personal experience of using Cao's method.

In this example, we shall show, for small differences of embedding dimension and delay of the same mixed signal, the general applicability of the proposed algorithm. The harmonic signal is generated by Eq. (38) with $A_k(j) = 0.00001 +$

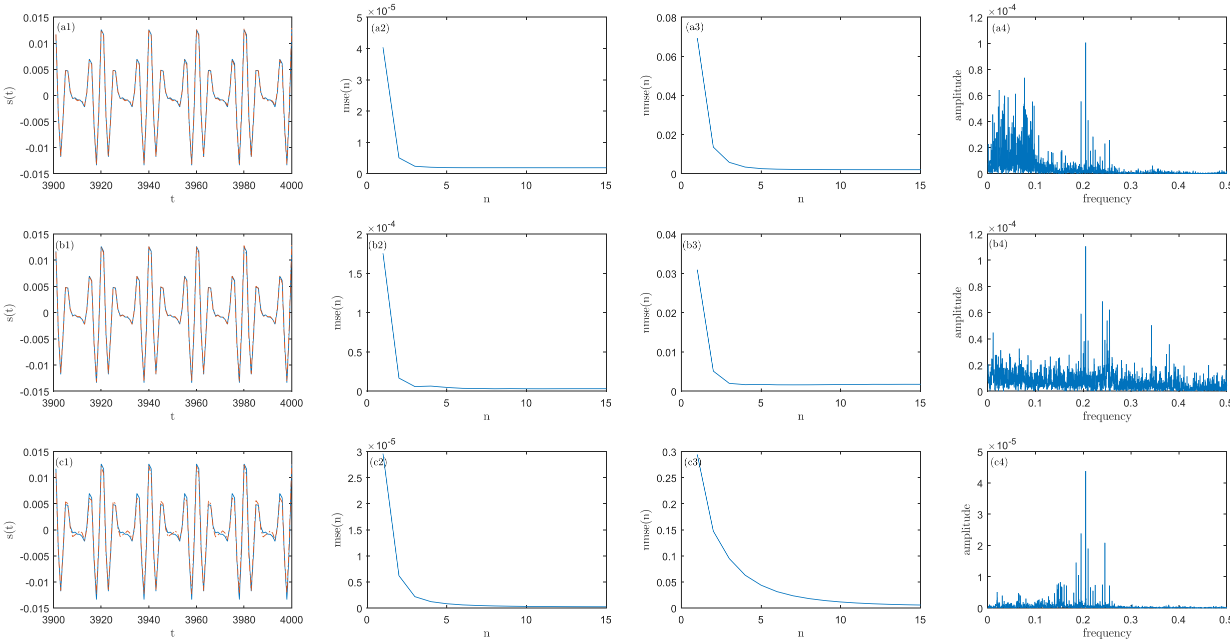

Fig. 9. Simulation results for Example 3: (a1) estimated harmonic signal (-·) with $(\omega_1, \omega_2, \omega_3) = (0.2501, 0.1501, 0.2001)$, together with the real harmonic signal (-); (a2) iteration's results of *mse* of the mixed Lorenz and harmonic signal with $(\omega_1, \omega_2, \omega_3) = (0.2501, 0.1501, 0.2001)$; (a3) iteration's results of *nmse* of harmonic signal with $(\omega_1, \omega_2, \omega_3) = (0.2501, 0.1501, 0.2001)$; (a4) periodograms of fitting error of the Lorenz and harmonic signal minus estimation of harmonic signal with $(\omega_1, \omega_2, \omega_3) = (0.2501, 0.1501, 0.2001)$; (b1)–(b3) and (c1)–(c3) display the results from the mixed harmonic and Henon, M–G signals, respectively.

$0.00001(5^{j-1} - 1)$, $j = 4, 5, 6$ and $k = 1, 2, 3$, and $W_1 \triangleq (\omega_1, \omega_2, \omega_3) = (0.25, 0.15, 0.2)$, $W_2 \triangleq (\omega_1, \omega_2, \omega_3) = (0.2501, 0.1501, 0.2001)$ are used for showing the performance of the original algorithm and its improved version. In Examples 2 and 3, we note that, for low accurate estimated frequencies, the performance of the original algorithm is bad. Thus, for low accurate estimated frequencies, we only use the advanced algorithm.

The extracted results with varied amplitude of different mixed signals are summarized in Tables 3–5, respectively. We use the original algorithm to estimate the harmonic signal with the accurate estimated frequencies and the advanced version to obtain the harmonic signal with the low accurate estimated frequencies. From Table 3, for the mixed Lorenz and harmonic signal, it can be seen that the harmonic signals are extracted well with both the two groups of frequencies. Indeed, we cannot deny that the performance of the improved version with the low accurate estimated frequencies are reduced than that of the accurate estimated frequencies and original algorithm. We can get the same conclusions for the other mixed signals from Tables 4 and 5, respectively.

4. Conclusions

In this paper, we are interested in detecting and extracting harmonic signal in strong chaotic background. Based on the short term predictability and sensitivity to initial value, we provide a new method. The proposed method first uses LL model's fitting error to detect the frequencies of harmonic signal by periodogram, a property is proposed which has not been addressed before. Then we enlarge the modeling capacity substantially. We establish a two-layer LL model to estimate the harmonic signal in strong chaotic background. To estimate this simply and effectively, we develop an efficient backfitting algorithm to select and optimize the parameters that are hard to be exhaustively searched for.

Given the conditions (**A1**)–(**A5**), the process of successive approximations is convergence. In the numerical experiments, three different chaotic signals are used as chaotic noise, and different harmonic signals are also used to test the proposed algorithm. From the simulation, it can be seen that the harmonic signal can be extracted well, the proper *SNR*s are shown for three different chaotic backgrounds. Example 1 shows that the frequencies of harmonic signal can be detected well. Example 2 shows that the two-layer LL model and its estimation technique have appreciable flexibility to model the determinate harmonic signal in different chaotic backgrounds. Specifically, the harmonic signal can be extracted well with low *SNR* and the developed background algorithm satisfies the condition of convergence in repeated 3–5 times. The characteristics of the initial iteration that mse_2 rapidly reduces and $nmse_1$ is very small are shown in Fig. 8. Furthermore, we investigate an improved technique for low accurate estimated frequencies in Example 3 and simulation shows that our technique is effective, which can help us to reduce searching time and improve accuracy of estimation of frequencies. From Examples 4 and 5, it can be seen that the two-layer LL model can extract harmonic signal well for different chaotic signals

Table 2
Simulation results for Example 4: varied amplitude.

SNR	Lorenz				*SNR*	Henon				*SNR*	M-G			
	W_1		W_2			W_1		W_2			W_1		W_2	
	mse	*nmse*	*mse*	*nmse*		*mse*	*nmse*	*mse*	*nmse*		*mse*	*nmse*	*mse*	*nmse*
−267.60	1.66e−6	3.71	1.65e−6	171	−220.76	1.05e−7	1.45e−2	2.51e−7	4.13	−225.28	1.03e−7	7.99	1.08e−7	409
−235.41	1.66e−6	0.15	1.65e−6	6.85	−188.57	1.00e−7	5.09e−4	2.50e−7	0.39	−193.09	1.04e−7	0.30	1.09e−7	17.3
−203.22	1.65e−6	6.24e−3	1.65e−6	0.28	−156.39	1.16e−7	1.08e−5	8.40e−7	1.13e−2	−160.90	1.03e−7	1.21e−2	1.09e−7	0.75
−171.03	1.64e−6	2.33e−4	1.66e−6	1.27e−2	−124.20	9.67e−8	1.72e−6	6.29e−7	3.07e−3	−128.71	9.99e−8	5.29e−4	1.16e−7	3.20e−2
−138.85	1.65e−6	1.00e−5	1.92e−6	2.04e−3	−92.01	1.25e−7	1.46e−8	2.90e−6	1.75e−3	−96.52	1.01e−7	1.77e−5	3.17e−7	4.28e−3
−106.66	1.67e−6	4.44e−7	6.17e−6	1.45e−3	−59.81	1.24e−5	5.37e−4	3.91e−5	1.70e−3	−64.36	7.55e−6	5.11e−3	1.37e−5	9.47e−3
−74.47	2.41e−6	1.69e−7	7.97e−5	1.55e−3	−27.63	2.17e−2	0.80	1.44e−2	0.58	−32.15	1.51e−3	0.93	1.39e−3	0.98
−42.28	2.79e−4	8.02e−2	1.91e−3	1.73e−3	4.56	2.79e−2	1.01	1.94e−2	1.03	0.04	4.58e−5	1.01	3.74e−5	1.00
−10.09	8.75e−2	1.13	8.86e−2	1.05	36.75	2.51e−3	1.00	2.04e−3	1.00	32.23	1.38e−4	1.00	1.11e−4	1.00

Table 3
Simulation results for Example 5: the mixed Lorenz and harmonic signal.

SNR		W_1			W_2		
	$m\backslash\tau$	6	7	8	6	7	8
−171.03	5	1.68e−6(8.89e−4)	1.91e−6(1.02e−3)	2.34e−6(2.98e−4)	1.66e−6(2.10e−2)	1.86e−6(1.66e−2)	2.33e−6(4.96e−2)
	6	1.26e−6(1.65e−4)	1.64e−6(2.33e−4)	2.31e−6(1.20e−3)	1.25e−6(2.93e−2)	1.66e−6(1.27e−2)	2.25e−6(5.04e−2)
	7	1.12e−6(4.96e−4)	1.73e−6(4.81e−4)	2.82e−6(6.16e−4)	1.11e−6(2.77e−2)	1.74e−6(2.18e−2)	2.52e−6(0.28)
−138.85	5	1.69e−6(3.09e−5)	2.08e−6(4.74e−5)	2.32e−6(2.96e−5)	1.85e−6(2.22e−3)	2.22e−6(1.99e−3)	2.47e−6(2.95e−3)
	6	1.26e−6(3.18e−6)	1.65e−6(1.00e−5)	2.32e−6(6.15e−5)	1.50e−6(2.46e−3)	1.92e−6(2.04e−3)	2.52e−6(4.01e−3)
	7	1.10e−6(2.06e−5)	1.72e−6(1.62e−5)	2.83e−6(2.94e−5)	1.43e−6(2.71e−3)	2.04e−6(2.57e−3)	2.70e−6(5.28e−3)
−106.66	5	2.84e−6(1.24e−6)	1.96e−6(1.48e−6)	2.53e−6(2.60e−6)	5.88e−6(1.43e−3)	6.25e−6(1.44e−3)	6.19e−6(1.47e−3)
	6	1.31e−6(2.61e−7)	1.67e−6(4.44e−7)	2.38e−6(4.12e−6)	5.62e−6(1.49e−3)	6.17e−6(1.45e−3)	7.34e−6(1.60e−3)
	7	1.12e−6(9.89e−7)	1.71e−6(4.85e−7)	2.81e−6(1.26e−6)	5.19e−6(1.54e−3)	6.86e−6(1.60e−3)	7.45e−6(1.91e−3)

Note: Number in parentheses represents *nmse* of the convergent iteration's results of harmonic signal; number out of the parentheses represents *mse* of the convergent iteration's results of the mixed signal. The same to below two tables.

Table 4
Simulation results for Example 5: the mixed Henon and harmonic signal.

SNR		W_1			W_2		
	$m\backslash\tau$	1	2	3	1	2	3
−124.20	3	1.38e−7(8.28e−6)	4.08e−5(1.70e−3)	9.40e−4(0.28)	5.93e−7(2.16e−3)	3.96e−5(0.13)	3.79e−4(1.21)
	4	9.67e−8(1.72e−6)	3.93e−4(1.00e−4)	6.39e−3(2.26)	6.29e−7(3.07e−3)	1.38e−4(2.74e−2)	3.12e−3(9.97)
	5	2.68e−7(2.41e−6)	3.84e−4(2.62e−5)	1.97e−2(0.33)	4.35e−6(2.89e−3)	7.82e−4(0.58)	1.22e−2(16.5)
−92.01	3	2.37e−7(3.67e−6)	9.85e−5(2.20e−4)	5.56e−4(5.08e−3)	2.47e−6(1.71e−3)	7.01e−5(1.73e−2)	2.52e−4(2.13e−2)
	4	1.25e−7(1.46e−8)	3.60e−4(2.17e−6)	3.79e−3(3.40e−2)	2.90e−6(1.75e−3)	3.40e−4(1.29e−2)	3.34e−3(0.35)
	5	2.92e−7(6.85e−8)	1.01e−3(3.35e−6)	1.24e−2(3.85e−5)	3.93e−6(2.10e−3)	1.21e−3(4.52e−2)	1.25e−2(0.86)
−59.81	3	4.20e−5(3.09e−3)	6.09e−4(2.53e−5)	2.17e−3(2.66e−3)	6.04e−5(3.72e−3)	5.88e−4(2.91e−3)	1.63e−3(4.94e−3)
	4	1.24e−5(5.37e−4)	1.72e−3(1.71e−7)	5.83e−3(1.68e−3)	3.91e−5(1.70e−3)	2.83e−4(2.61e−3)	4.53e−3(1.51e−2)
	5	1.59e−6(2.37e−7)	2.82e−3(7.00e−5)	1.51e−2(3.25e−4)	3.90e−5(1.69e−3)	1.62e−3(7.33e−3)	1.22e−2(4.97e−2)

Table 5
Simulation results for Example 5: the mixed M–G and harmonic signal.

SNR		W_1			W_2		
	$m\backslash\tau$	5	6	7	5	6	7
−128.71	5	8.77e−8(5.01e−5)	1.27e−7(2.62e−4)	1.64e−7(4.56e−5)	9.57e−8(7.07e−3)	1.33e−7(2.03e−2)	1.76e−7(1.38e−2)
	6	6.31e−8(2.13e−4)	9.99e−8(5.29e−4)	8.00e−8(1.90e−5)	9.01e−8(1.83e−2)	1.16e−7(3.20e−2)	9.05e−8(2.78e−3)
	7	5.76e−8(2.30e−4)	6.01e−8(1.98e−4)	3.86e−8(4.29e−5)	7.26e−8(1.25e−2)	7.17e−8(1.09e−2)	5.14e−8(3.17e−3)
−96.52	5	9.89e−8(1.85e−6)	1.50e−7(1.55e−5)	2.00e−7(4.12e−6)	3.15e−7(3.41e−3)	3.17e−7(2.57e−3)	4.70e−7(2.72e−3)
	6	6.51e−8(1.53e−5)	1.01e−7(1.77e−5)	8.37e−8(1.96e−6)	3.18e−7(6.21e−3)	3.17e−7(4.28e−3)	3.13e−7(2.03e−3)
	7	5.86e−8(1.23e−5)	6.51e−8(1.18e−5)	4.25e−8(3.21e−6)	3.59e−7(6.65e−3)	2.69e−7(3.01e−3)	2.71e−7(2.81e−3)
−64.36	5	1.61e−6(1.45e−3)	1.22e−5(1.18e−2)	5.41e−6(1.67e−3)	6.01e−6(3.36e−3)	2.08e−5(2.03e−2)	1.18e−5(4.92e−3)
	6	7.51e−7(4.09e−4)	7.55e−6(5.11e−3)	1.85e−6(3.46e−4)	4.47e−6(2.12e−3)	1.37e−5(9.47e−3)	6.41e−6(2.25e−3)
	7	5.04e−7(1.98e−5)	1.48e−6(6.47e−4)	6.68e−7(8.50e−5)	4.43e−6(1.87e−3)	7.50e−6(4.44e−3)	4.56e−6(2.35e−3)

with different embedding dimensions and delays. The estimated frequencies of sine signal with low accuracy dissatisfies condition (**A1**) and the optimization objectives (Eqs. (25) and (23)) have slightly large difference. This explains the slightly large *nmse*s with low accuracy estimated frequencies in Tables 3–5. The two-layer LL model is exhaustively researched and successfully applied for extracting the harmonic signal in strong chaotic signal background. Indeed, this depends on the prerequisite that the chaotic noise can be approximated well by LL model. And the performance of detecting frequencies from fitting error by periodogram is another restricted factor for extracting harmonic signal.

References

[1] H. Leung, Chaotic Signal Processing, Higher Education Press, Beijing, China, 2014.
[2] J. Stark, B.V. Arumugam, Extracting slowly varying signals from a chaotic background, Int. J. Bifurc. Chaos 2 (02) (1992) 413–419, http://dx.doi.org/10.1142/S0218127492000409.
[3] S. Haykin, B.X. Li, Chaotic detection of small target in sea clutter, in: IEEE International Conference on Acoustics, Speech, and Signal Processing, vol. 1, 1993, pp. 237–240. http://dx.doi.org/10.1109/ICASSP.1993.319099.
[4] H. Leung, T. Lo, Chaotic radar signal processing over the sea, IEEE J. Ocean. Eng. 18 (1993) 287–295, http://dx.doi.org/10.1109/JOE.1993.236367.
[5] S. Haykin, B.X. Li, Detection of signals in chaos, Proc. IEEE 83 (1) (1995) 95–122, http://dx.doi.org/10.1109/5.362751.
[6] H. Leung, X.P. Huang, Parameter estimation in chaotic noise, IEEE Trans. Signal Proc. 44 (10) (1996) 2456–2463, http://dx.doi.org/10.1109/78.539030.
[7] K.M. Short, Signal extraction from chaotic communications, Int. J. Bifurc. Chaos 7 (07) (1997) 1579–1597, http://dx.doi.org/10.1142/S0218127497001230.
[8] X.Y. Ma, X.B. Huang, F. Wang, X.D. Xu, A new method for small target detection over chaotic background, in: IEEE CIE International Conference on Radar Proceedings, 2001, pp. 341–344. http://dx.doi.org/10.1109/ICR.2001.984689.
[9] Z.W. Zhu, H. Leung, Identification of linear systems driven by chaotic signals using nonlinear prediction, IEEE Trans. Circuits Syst. I: Fund. Theory Appl. 49 (2-C49) (2002) 170–180, http://dx.doi.org/10.1109/81.983865.
[10] Y. Li, B. Yang, Chaotic system for the detection of periodic signals under the background of strong noise, Chin. Sci. Bull. 48 (5) (2003) 508–510, http://dx.doi.org/10.1007/BF03183261.
[11] E. Wang, Q. Liu, L. Jia, Q. Ding, A steady-state point capture-based blind harmonic signal extraction algorithm under the chaotic background, Int. J. Sens. Netw. 15 (1) (2014) 52–61, http://dx.doi.org/10.1504/IJSNET.2014.059992.
[12] H.L. Zheng, H.Y. Xing, W. Xu, Detection of weak signal embedded in chaotic background using echo state network, Signal Process 31 (3) (2015) 336–345, http://dx.doi.org/10.3969/j.issn.1003-0530.2015.03.012. (in Chinese).
[13] G. Wang, J. Lin, X. Chen, The application of chaotic oscillators to weak signal detection, IEEE Trans. Ind. Electron. 46 (2) (1999) 440–444, http://dx.doi.org/10.1109/41.753783.
[14] G. Wang, W. Zheng, S. He, Estimation of amplitude and phase of a weak signal by using the property of sensitive dependence on initial conditions of a nonlinear oscillator, Signal Proc. 82 (1) (2002) 103–115, http://dx.doi.org/10.1016/S0165-1684(01)00166-9.
[15] Q.Z. Liu, W.Q. Song, Detection weak period signal using chaotic oscillator, in: Computer Science and Its Applications (ICCSA 2009), 2009, pp. 685–692. http://dx.doi.org/10.1007/978-3-642-02454-2_51.
[16] X. Deng, H. Liu, L. Wang, T. Liu, Study on detection of small-sized range-spread target by using chaotic duffing oscillator, in: IEEE Conference on Anthology, 2013, pp. 1–4. http://dx.doi.org/10.1109/ANTHOLOGY.2013.6784845.
[17] L.Y. Su, C.L. Li, Local functional coefficient autoregressive model for multistep prediction of chaotic time series, Discret. Dyn. Nat. Soc. 2015 (2) (2015) 1–13, http://dx.doi.org/10.1155/2015/329487.
[18] L.Y. Su, C.L. Li, Local prediction of chaotic time series based on polynomial coefficient autoregressive model, Math. Probl. Eng. 2015 (2) (2015) 1–14, http://dx.doi.org/10.1155/2015/901807.
[19] J.D. Farmer, J.J. Sidorowich, Predicting chaotic time series, Phys. Rev. Lett. 59 (8) (1987) 845–848, http://dx.doi.org/10.1103/PhysRevLett.59.845.
[20] F. Takens, Dynamical systems and turbulence, in: Lecture Notes in Mathematics, vol. 898, no. 9, 1981, pp. 366–381. http://dx.doi.org/10.1142/9789812792822_0030.
[21] L. Cao, Practical method for determining the minimum embedding dimension of a scalar time series, Phys. D: Nonlinear Phenom. 110 (1) (1997) 43–50, http://dx.doi.org/10.1016/S0167-2789(97)00118-8.
[22] J.Q. Fan, Z.W. Cai, Adaptive varying-coefficient linear models, J. R. Stat. Soc. B 65 (1) (2003) 57–80, http://dx.doi.org/10.1111/1467-9868.00372.
[23] E.N. Lorenz, Deterministic non-periodic flow, J. Atmos. Sci. 20 (2) (1963) 130–141, http://dx.doi.org/10.1007/978-0-387-21830-4_2.
[24] M. Henon, Y. Pomeau, Two Strange Attractors with a Simple Structure, Springer, Berlin, Heidelberg (1976), pp. , 1976, 29–68, http://dx.doi.org/10.1007/BFb0091446.
[25] M. Mackey, L. Glass, Oscillation and chaos in physiological control systems, Science 197 (4300) (1977) 287–289, http://dx.doi.org/10.1126/science.267326.